JOURNAL OF GEOPHYSICAL RESEARCH, VOL. 104, NO. D21, PAGES 26,581–26,595, NOVEMBER 20, 1999

Empirical age spectra for the lower tropical stratosphere from in situ observations of CO_2: Implications for stratospheric transport

A. E. Andrews,[1] K. A. Boering,[1,2], B. C. Daube,[1] S. C. Wofsy,[1] E. J. Hintsa,[3,4]
E. M. Weinstock,[3] and T. P. Bui[5]

Abstract. Empirical age spectra for the lower tropical stratosphere (from the tropopause to ~19.5 km) have been derived from in situ measurements of CO_2, using information provided by the vertical propagation of the tropospheric seasonal cycle and long-term positive trend. Our method provides accurate and unambiguous mean ages for this region which are difficult to obtain by simple analysis of lag times from tracer measurements. We find that the air is 30-40% younger in northern spring than in autumn. For example, at 460 K the mean age (relative to the tropical tropopause) was 0.4 years in March and 0.6 years in September. The phase lag times and attenuation of CO_2 seasonal extrema in the stratosphere are shown to depend on seasonal variations in transport rates and on the presence of harmonics in the CO_2 boundary condition with frequencies higher than 2π/yr. Profiles of stratospheric water vapor, generated from the derived age spectra with a stratospheric boundary condition based on observed tropical tropopause temperatures, are consistent with in situ observations of H_2O. Comparison of the predicted water vapor seasonal cycle with satellite observations suggests that satellite-borne instruments underestimate the amplitude near the tropical tropopause. We relate the empirical age spectra to the analytic solution for the 1-D advection-diffusion tracer continuity equation to obtain seasonally resolved estimates of the ascent rate and the vertical diffusion coefficient. The derived age spectra provide a unique observation-based diagnostic for evaluating the simulation of tracer transport in models.

1. Introduction

The composition of the stratosphere depends sensitively on transport rates for contaminants such as CFCs, exhaust from high-flying aircraft, and aerosols from volcanic eruptions. The general characteristics of the stratospheric circulation are well known: air enters through the tropical tropopause, ascends in the tropics, and descends at middle and high latitudes, eventually returning to the troposphere [*Brewer*, 1949; *Dobson*, 1956; *Holton et al.*, 1995]. However, present knowledge of rates for advection and diffusion in the stratosphere is inadequate for quantifying natural and anthropogenic perturbations to the ozone layer [*Graedel*, 1994; *Stolarski et al.*, 1995].

Quantitative information on rates for tracer transport in the region just above the tropical tropopause is particularly important for understanding tracer distributions throughout the stratosphere. For example, global lifetimes for CFCs and N_2O depend critically on the relative rates for vertical and horizontal transport in this region. The mean vertical velocity in the tropics provides a direct measure of the turnover time for the entire stratosphere, and rates of exchange between this tropical upwelling region and higher latitudes regulate dispersal of pollutants such as exhaust from stratospheric aircraft.

Rates for vertical advection, quasi-horizontal mixing with air from midlatitudes, and vertical diffusion in the tropics have recently been estimated from satellite measurements, showing the propagation and attenuation of the seasonal cycle in $H_2O + 2*CH_4$ [*Mote et al.*, 1995, 1996, 1998; *Hall and Waugh*, 1997b]. Vertical velocities have also been computed using radiative transfer models and satellite observations of temperature, cloud cover, and ozone [*Rosenlof*, 1995; *Eluszkiewicz et al.*, 1996]. Unfortunately, the accuracy and resolution of available satellite data decline below 50 hPa [e.g., *Mote et al.*, 1998], and net heating rates for the near-tropopause region are calculated from small differences between large numbers [see *Rosenlof*, 1995; *Volk*, 1996]. These factors make it difficult to derive transport information from satellite observations near the tropopause, where much of the exchange between the tropics and higher latitudes is thought to occur [e.g., *Trepte and Hitchman*, 1992; *Boering et al.*, 1994, 1996; *Volk et al.*, 1996; *Mote et al.*, 1996, 1998; *Herman et al.*, 1998].

In situ tracer data can potentially provide detailed information on transport in the critical region below 50 hPa (~21 km) in the tropical stratosphere. Exchange rates between the tropics and the midlatitudes have recently been estimated from

[1]Department of Earth and Planetary Sciences and the Division of Engineering and Applied Sciences, Harvard University, Cambridge, Massachusetts.
[2]Now at Departments of Chemistry and of Geology and Geophysics, University of California, Berkeley.
[3]Department of Chemistry and Chemical Biology, Harvard University, Cambridge, Massachusetts.
[4]Now at Department of Marine Chemistry and Geochemistry, Woods Hole Oceanographic Institution, Woods Hole, Massachusetts.
[5]NASA Ames Research Center, Moffett Field, California.

Paper number 1999JD900150.
0148-0227/99/1999JD900150$09.00

analyses of measurements of ozone and of trace species originating in the troposphere that are removed photochemically in the stratosphere (e.g., N_2O, CH_4, and the CFCs) [*Avallone and Prather*, 1996; *Minschwaner et al.*, 1996; *Volk et al.*, 1996]. Vertical velocities were estimated from analysis of the propagation of seasonal extrema observed in tropical CO_2 profiles [*Boering et al.*, 1996]. In general, however, studies based on in situ observations have been constrained by sparse data covering a limited altitude range. In particular, the data available could not completely constrain the vertical velocities and mixing rates, generally requiring introduction of vertical velocities computed from radiative codes [e.g., *Volk et al.*, 1994] and, except for *Boering et al.* [1996], could not resolve seasonal variations.

Observations of stratospheric CO_2 obtained from 1992 to 1997 over an extensive range of altitudes, latitudes, and seasons show the propagation of temporal variations from the troposphere into the stratosphere [*Boering et al.*, 1994, 1995, 1996]. Tropospheric CO_2 concentrations have been increasing due to fossil fuel combustion, with an average growth rate over the past several decades of 1.5 ppmv/yr. Seasonal cycles are superimposed on this long-term trend due to uptake and release by the terrestrial biosphere [*Keeling et al.*, 1989; *Conway et al.*, 1994]. At the surface the seasonal cycle varies with latitude, with the largest amplitudes observed at high latitudes in the Northern Hemisphere (NH). Measurements showing the propagation and attenuation of the seasonal cycle and long-term positive trend into the stratosphere provide insight into transport processes occurring over both short (weeks-months) and long (years) timescales. CO_2 has no significant sinks in the stratosphere and only a small source from oxidation of CH_4 that is easily taken into account using simultaneous CH_4 observations.

In this paper we present empirical age spectra for the lower tropical stratosphere (from the tropopause to ~19.5 km) derived from observations of stratospheric CO_2. The age spectrum for a stratospheric air parcel represents the statistical distribution of transit times from the tropopause for the ensemble of irreducible fluid elements comprising the parcel [*Hall and Plumb*, 1994]. Age spectra therefore reflect the aggregated effects of advective and diffusive processes transporting trace species in the stratosphere. An age spectrum is mathematically equivalent to the Green's function, which generates the time series of mixing ratios for a conserved tracer at a point in the stratosphere when convolved with the time series at the lower boundary (the equatorial tropopause). We examine the derived age spectra using the analytic solution for the Green's function for the one-dimensional (1-D) advection-diffusion equation to obtain estimates of vertical ascent rates and effective vertical diffusion coefficients. We also show that profiles of water vapor mixing ratios generated using the derived age spectra with a stratospheric boundary condition based on tropical tropopause temperatures are consistent with in situ observations, lending support to our results as well as to the proposed water vapor boundary condition.

Hall and Plumb [1994] and *Hall and Waugh* [1997a] have demonstrated the value of age spectra as tools for interpreting tracer data and for comparing transport parameterizations among numerical models of the atmosphere. Several previous studies have shown that observations of CO_2 and SF_6, both of which have been increasing at roughly constant rates over the past several decades, can be used to determine the mean age Γ, which represents the average transit time for an air parcel from a reference point (either the surface or the tropical tropopause) to the location of the measurement [e.g., *Bischof et al.*, 1985; *Schmidt and Khedim*, 1991; *Boering et al.*, 1996; *Harnisch et al.*, 1996; *Elkins et al.*, 1996]. The present study is, to our knowledge, the first attempt to obtain information about the age spectrum beyond the mean age using atmospheric observations of trace species.

2. Observations

Measurements of CO_2 mixing ratios were made on the NASA ER-2 aircraft up to 21 km by nondispersive infrared absorption and were calibrated in flight with a long-term precision (i.e., flight to flight and year to year) of $\pm$ 0.1 ppmv [*Boering et al.*, 1994, 1996]. Field campaigns included the Stratospheric Photochemistry and Dynamics Expedition (SPADE, 1992-1993, 14°N to 61°N), the Airborne Southern Hemisphere Ozone Experiment/Measurements for Assessing the Effects of Stratospheric Aircraft (ASHOE/MAESA, 1994, 70°S to 61°N), Stratospheric Tracers of Atmospheric Transport (STRAT, 1995-1996, 3°S to 61°N), and Photochemistry of Ozone Loss in the Arctic Region in Summer (POLARIS, 1997, 2°S to 90°N). We focus here on seven vertical profiles obtained in the tropical upwelling region from 1994 to 1997 between the tropopause and ~19.5 km (symbols in Figure 1). We account for CH_4 oxidation using simultaneous measurements from the Airborne Laser Infrared Absorption Spectrometer (ALIAS) [*Webster et al.*, 1994], assuming that the difference between the measured CH_4 mixing ratios and the tropospheric value ($\cong$ 1700 ppb) represents the quantity of CH_4 oxidized to CO_2. For the altitude and latitude ranges considered here, the magnitude of this correction is small (< 0.1 ppmv).

The latitude range selected for each flight varied from 5°S to 5°N for the October 1994 flights to 2°S to 3.5°N for the February 1996 flight, usually limited on the southern end by the range of the ER-2 when based in Hawaii (20°N). In general, we chose 5°N as the northerly cutoff. However, some data in this latitude range were omitted from the profiles for March 1994, February 1996, August 1996, and December 1996 (light symbols in Figure 1) corresponding to times when the aircraft encountered filaments of air recently transported from higher latitudes, as indicated by simultaneously measured tracers such as N_2O, O_3, NO_y, and the CFCs. Observations of such filaments may provide insight into the mechanism(s) of exchange between the tropics and the extratropics, but they are excluded from this analysis in order to focus on the integrated mean distribution of transit times. Tropical CO_2 profiles are especially sensitive to admixture of air from higher latitudes because the amplitude of the seasonal cycle is smaller than changes in CO_2 associated with the long-term trend for air older than ~1 year.

A continuous representation of the stratospheric boundary condition for CO_2 is required in order to derive empirical age spectra from the observed profiles of CO_2 in Figure 1. Air that had recently entered the stratosphere was sampled when the aircraft flew near the tropical tropopause, the primary entry point for the stratospheric overworld. However, the tropical observations alone do not sufficiently define the stratospheric boundary condition. Fortunately, we have also measured CO_2 mixing ratios in air that has recently entered the stratosphere when tropical filaments were encountered in the extratropics [*Boering et al.*, 1994, 1996]. New stratospheric

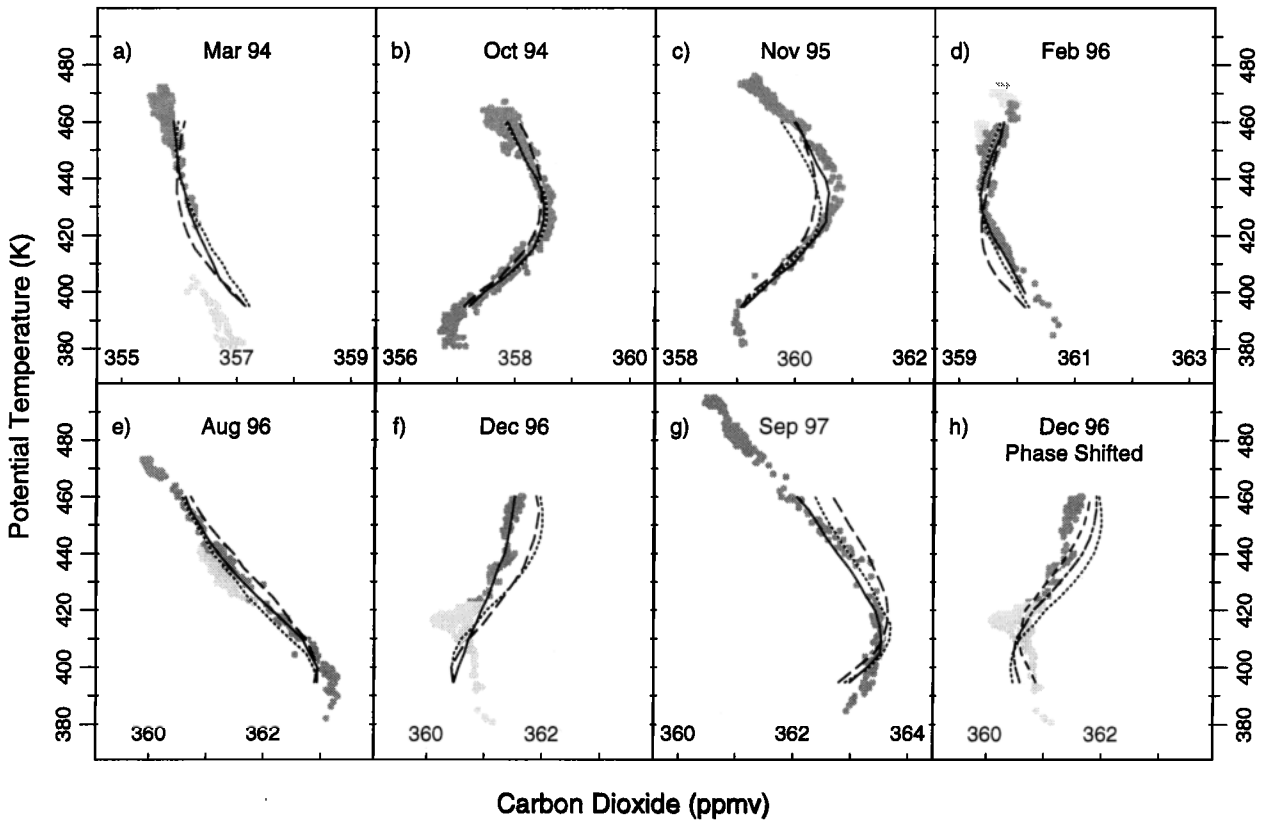

Figure 1. (a-g) Vertical profiles of CO_2 (corrected for CH_4 oxidation; see text) obtained from 1994 to 1997 on the NASA ER-2 aircraft between 5°S and 5°N. The lighter points were not included in this analysis due to evidence of extratropical filaments in simultaneous measurements of N_2O, O_3, NO_y, and CFCs. Solid lines correspond to the optimum Γ and τ_M profiles for each flight. Dotted lines correspond to the fits to Γ and τ_M shown in Plate 1, and dashed lines represent annually averaged Γ and τ_M profiles. (h) Sensitivity of the solution for December 1996 to the phase of the boundary condition. The dotted line corresponds to the seasonally varying fits to Γ and τ_M with the unmodified boundary condition (same as dotted line in Figure 1f), the dotted-dashed and dashed lines correspond to phase delays in the boundary condition of 2 weeks and 1 month, respectively.

air was identified by near-tropospheric N_2O mixing ratios (≅310 ppb), high CO mixing ratios (30-45 ppb), and potential temperatures ≥ 390 K. Filaments with these characteristics were encountered at both northern and southern extratropical latitudes in all seasons except Southern Hemisphere summer, for which there is no ER-2 CO_2 data to date. These data, along with measurements obtained near the tropical tropopause, provide 24 observations of the stratospheric boundary condition for CO_2 (Figure 2) for 17 distinct time periods from 1992 to 1997. On the seven occasions when new stratospheric air was observed both in the tropics and in the tropical filaments at higher latitudes, there is very close agreement in the CO_2 mixing ratio, verifying that little or no modification of the CO_2 mixing ratios in the filaments had occurred during transport from the tropics.

Boering et al. [1996] noted that the observations of the CO_2 boundary condition are phenomenologically well represented by the average of ground-based CO_2 mixing ratio data from Mauna Loa (19°N) and Samoa (14°S) delayed by two months. However, there remains some uncertainty at the times of the seasonal extrema, and there are not enough data to determine both the seasonal cycle and the interannual variations in the growth rate. We obtained an estimate of the long-term trend (dashed line in Figure 2a) by removing the seasonal cycle from the Mauna Loa/Samoa index using a 12-month running mean. We subtracted this result from the observations of the boundary condition to isolate the seasonal variation and then calculated an average seasonal cycle for 1992-1997 by fitting a function with annual and semiannual harmonics to the residuals (Figure 2b). The seasonal cycle derived in this manner for air entering the stratosphere has a peak-to-peak amplitude of 3.2 ppmv with a maximum in early July and a minimum in mid-November, consistent with flask measurements of CO_2 in the upper tropical troposphere [Nakazawa *et al.*, 1991; *Matsueda* and *Inoue*, 1996]. The sum of the long-term trend and the average seasonal cycle (solid line in Figure 2a) provides a continuous representation of the stratospheric boundary condition. We consider the sensitivity of our results to potential errors in this boundary condition in section 5.1.

In situ measurements of lower-stratospheric water vapor were obtained simultaneously with the CO_2 data by two different Lyman–α hygrometers. Data for March and October 1994 (ASHOE/MAESA) were obtained using an instrument from the NOAA Aeronomy Laboratory with a stated accuracy of 6% [*Kley et al.*, 1983]. Data for STRAT (October 1995

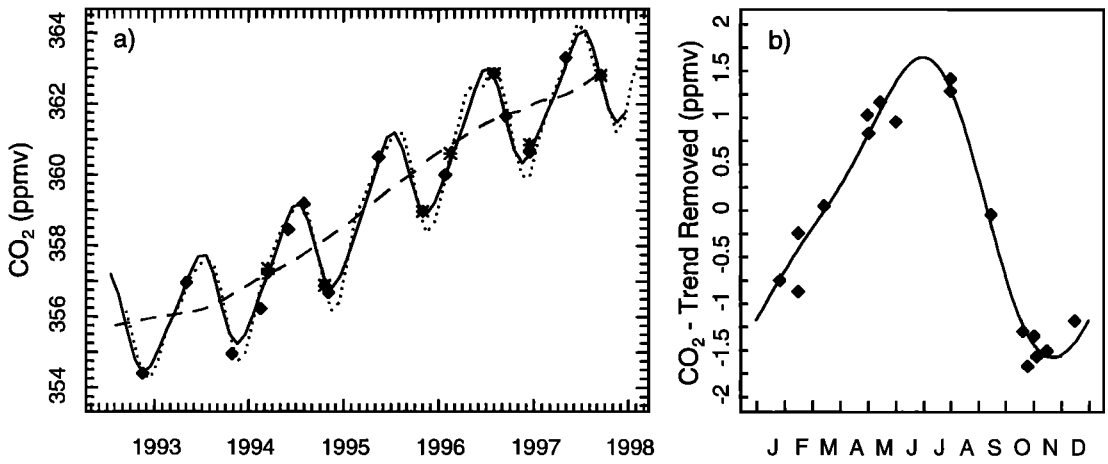

Figure 2. (a) Boundary condition for CO_2 entering the stratosphere. Data obtained in the tropics are shown as asterisks, while the diamonds represent data collected when the ER-2 aircraft intercepted an air mass with tropical character in the extratropics. The dotted curve is the average of surface data from the National Oceanic and Atmospheric Administration (NOAA) Climate Monitoring and Diagnostics Laboratory (CMDL) flask network stations at Mauna Loa (MLO) and Samoa (SMO) [*Conway et al.*,1994, updated] delayed by 2 months; the dashed line is the 12-month running mean of this MLO/SMO index; and the solid line is the sum of the dashed line and the two-harmonic fit to the detrended points shown in Figure 2b. (b) Points are the data shown in Figure 1a detrended by subtracting the 12-month running mean of the MLO/SMO index (dashed line in Figure 2a) and plotted versus time of year. The line is a fit with annual and semiannual harmonics given by $CO_2^{seas} = 0.007 + 1.490 \sin(2\pi t - 1.244) + 0.328 \sin(4\pi t + 0.766)$ where t is time in years.

and February, August, and December 1996) and POLARIS (September 1997) were obtained using the Harvard University H_2O instrument, with a stated accuracy of 5% [*Weinstock et al.*, 1994; *Hintsa et al.*, 1999]. The two instruments have been flown simultaneously, agreeing to ~15%, with the Harvard instrument consistently measuring higher concentrations.

3. Theory

The concept of the atmospheric age spectrum was introduced by *Kida* [1983] and developed by *Hall and Plumb* [1994] and *Hall and Waugh* [1997a]. The time series of tracer mixing ratio n at a location P in the stratosphere is related to the time series at the source region P_o by

$$n(P,t) = \int_0^t n(P_o, t-t')G(t,t',P;P_0)dt' \qquad (1)$$

where $G(t,t',P;P_o)$ is the age spectrum at point P and time t. Most air enters the stratosphere in the tropics, thus P_o corresponds to the equatorial tropopause. Here we consider exclusively the stratospheric overworld described by *Holton et al.* [1995], with potential temperature Θ greater than 390 K. G provides the statistical distribution function for the ensemble of transit times of air parcels from the tropical tropopause to point P; it is the Green's function that relates the mixing ratio $n(P,t)$ for any inert tracer to the time series of mixing ratio at the tropical tropopause via equation (1). Previous studies based on model-generated age spectra have only considered annual mean spectra, but we have made allowance for seasonal variations as required to account for important features of the observations.

Age spectra are typically described in terms of the spectral modal time, the mean age, and the spectral width. The spectral modal time τ_M is the most probable transit time and corresponds to the maximum of the Green's function. The mean age Γ is the first moment of the age spectrum:

$$\Gamma(P,t;P_o) = \int_0^\infty t'G(t,t',P;P_o)dt' \qquad (2)$$

Note that in this paper, Γ refers to stratospheric mean ages computed relative to P_o, at the tropical tropopause, not at the surface. For inert tracers that increase approximately linearly with time, such as SF_6, or CO_2 at altitudes where the seasonal cycle has been damped out, the mean age is equal to the lag time between occurrence of a given mixing ratio at the tropical tropopause and the same mixing ratio at location P [*Hall and Plumb*, 1994]. The spectral width Δ is the square root of the second moment about the mean,

$$\Delta^2(P,t;P_o) = \tfrac{1}{2}\int_0^\infty (t'-\Gamma(P,t;P_o))^2 G(t,t',P;P_o)dt' . \qquad (3)$$

Our results, described below, indicate that for the very young air in the lower tropical stratosphere, the age spectrum is adequately determined by knowledge of the mean age and the modal time (i.e., the width is essentially invariant for a given Γ:τ_M pair). Another important property of an age spectrum is the characteristic phase lag time τ_ω for a sinusoidally varying tracer. In a purely advective atmosphere, the mean age, modal time, and phase lag time would all be equal. Differences among these quantities thus reflect diffusive stratospheric transport such as vertical mixing and quasi-horizontal mixing along isentropes.

The unique temporal variations in CO_2, the long-term precision and frequency of the in situ measurements, and the well-defined boundary condition, make CO_2 an ideal tracer

for determining both Γ and τ_M and therefore the age spectrum in regions of the atmosphere where the seasonal cycle has not been damped out. For example, if we propose an age spectrum at a given altitude with a mean age that is too old, the corresponding time series of predicted CO_2 mixing ratios will have a lower mean value than observed. If the proposed age spectrum is too broad (i.e., Δ is too large), the CO_2 seasonal cycle in the resulting time series will be more attenuated than observed. The phase of the seasonal cycle further constrains both mean age and modal time. In contrast, the concentration of a tracer increasing linearly with time, with no seasonal cycle (e.g., SF_6), depends only on the mean age Γ and can therefore only be used to determine the first moment of the distribution function [*Hall and Plumb*, 1994]; there is no information about the width of the age spectrum. Conversely, observations of a periodically varying tracer with no significant long-term trend (e.g., H_2O + 2*CH_4) contain information about the width of the age spectrum but do not allow determination of the mean value of the distribution function.

4. Analysis

The basis of our analysis is to invert equation (1) to find the best fit solution for $G(t, t', P, P_o)$ given data for $CO_2(P, t)$ and $CO_2(P_o, t)$. At a particular altitude, the temporal resolution of the data (seven time points between March 1994 and September 1997) is inadequate to completely define the age spectrum. However, knowledge of the mixing ratios as a function of altitude provides sufficient additional information about the phase and amplitude of the seasonal cycle to remove most of the ambiguity. Consideration of the profiles acquired nearly one year apart in late October 1994 and early November 1995 allows us to test the reproducibility of our analysis.

We represent the age spectrum using the functional form

$$G(t,t',\theta;\theta_o) = \frac{A(\theta,t)}{\sqrt{t'^3}}\exp\left(-B(\theta,t)t' - \frac{C(\theta,t)}{t'}\right) \qquad (4)$$

where θ is potential temperature above the tropopause ($\theta = \Theta$ - 390 K). Potential temperature (Θ) was adopted as the vertical coordinate because it is conserved for adiabatic motion and therefore minimizes the impact of variations associated with reversible displacements of tracer surfaces [*Ehhalt*, 1983]. Equation (4) has the form of the analytic solution for the Green's function for the 1-D diffusion equation in the atmosphere [*Hall and Plumb*, 1994]. This form also fits most age spectra generated by 2-D and 3-D models reasonably well (T. M. Hall and D. W. Waugh, personal communication, 1998), indicating that its usefulness extends beyond the 1-D framework.

The Green's function is defined to have unit area, hence there are two independent parameters in equation (4), $B(\theta,t)$ and $C(\theta,t)$. This implies that for a particular θ and t, G is completely specified by any two of Γ, τ_M, and Δ. Because we had no a priori knowledge of the variation of B and C with θ and t, we worked instead with Γ and τ_M, which are expected to increase smoothly and monotonically with increasing altitude in the lower tropical stratosphere. Given candidate values for Γ and τ_M at a particular θ and t, equation (4) can be inverted to obtain a unique pair of corresponding coefficients B and C. According to equation (1) the resulting age spectrum can be convolved with a tracer boundary condition to obtain the tracer mixing ratio at θ and t. We examined the sensitivity of our results to the functional form of equation (4) by allowing the power of the term outside the exponential to vary. For the rather young air in the lower tropical stratosphere, this term had no effect on the inversion procedure for specified values of Γ and τ_M, indicating that the age spectrum is adequately determined by two parameters.

We performed a Monte Carlo analysis to identify profiles of Γ and τ_M, which best reproduced each of the observed CO_2 profiles in Figure 1. We chose a Monte Carlo approach so that we could determine whether more than one family of solutions reproduced the observations and to facilitate defining near-optimum solutions for nonlinear parameters. A random number generator was used to produce profiles of Γ and τ_M varying quadratically with potential temperature, assuming an intercept of zero years at the tropical tropopause (390 K) and requiring that Γ and τ_M increase monotonically with altitude. An upper limit on Γ of 1 year at 460 K was imposed on the basis of preliminary analysis of CO_2 mixing ratios as a function of Γ and τ_M. For each flight date, CO_2 mixing ratios were calculated using the boundary condition shown in Figure 2a for 2000 pairs of Γ and τ_M profiles at 14 equally spaced potential temperature surfaces ranging from 395 to 460 K. The root-mean-square difference between calculated and observed CO_2 was used to select the 15 pairs of Γ and τ_M profiles which best reproduced each observed CO_2 profile. Optimum Γ and τ_M profiles for each flight date were obtained by calculating the median value for this set on each isentrope. The results are plotted versus time of year in Plate 1 for 420, 440, and 460 K, and the corresponding CO_2 profiles are shown in Figure 1 (solid lines). The solutions obtained from this optimization were unambiguous for five flight dates, but the results for March 1994 and December 1996 require additional consideration.

For March 1994, two distinct families of Γ and τ_M profiles provided near-optimum solutions. One set was characterized by mean ages of 0.2 to 0.3 years and the other by mean ages of ~0.8 to 1 year (not shown) at 460 K. Both solutions had very short modal times. The explanation for this behavior is simple: addition of old air from midlatitudes attenuates a seasonal maximum in CO_2 but may enhance a minimum, which therefore appears less attenuated. If a profile contains a maximum or a region where CO_2 increases with increasing altitude, the solutions are tightly constrained. In March 1994, however, CO_2 decreased with altitude over the entire altitude range. In this case, the solution with older mean age results from addition of old air, while the solution with younger mean age is associated with the preservation and propagation of the seasonal minimum. The solution with younger mean age is much more consistent with the solutions obtained for the other flights, and we therefore conclude that the other solution is spurious.

For December 1996 the optimum modal time profile seems inconsistent with those obtained for the other flights. Close examination of Figure 2 reveals some discrepancy between the "newest air" data for December 1996 and the representation of the boundary condition. Profiles of Γ and τ_M for this flight can be brought into agreement with those obtained from the other flights by shifting the timing of the seasonal minimum in the boundary condition by 2-4 weeks as illustrated in Figure 1h. It appears that results for this flight are especially sensitive to small uncertainties in the boundary condition due

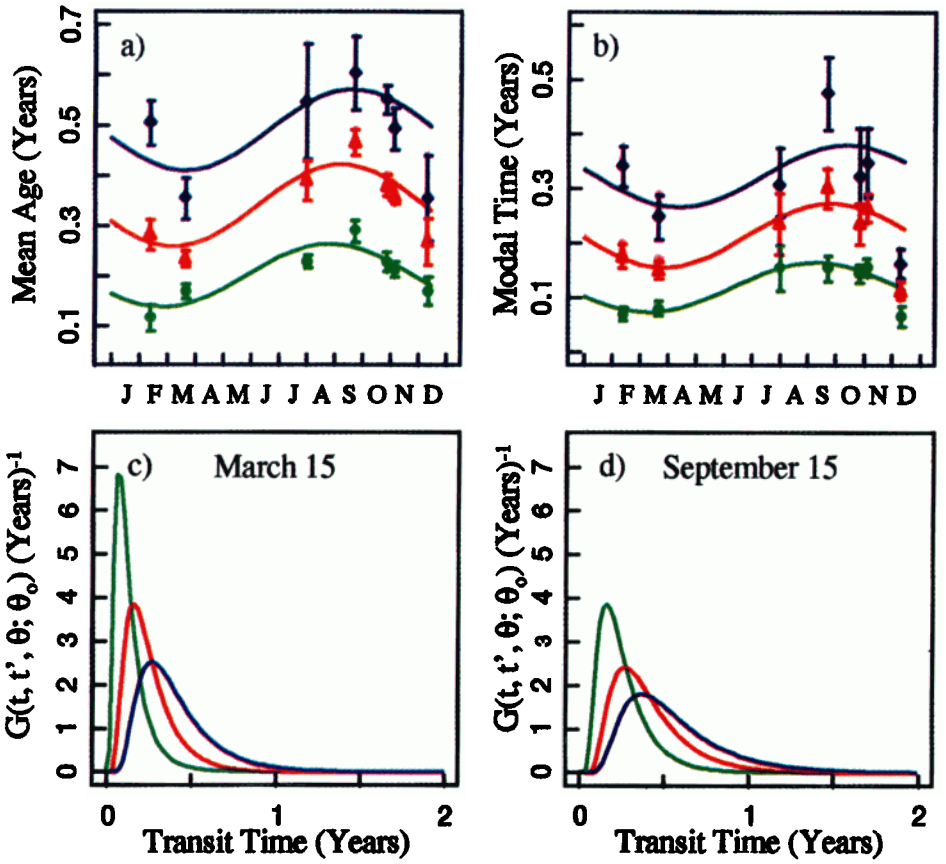

Plate 1. (a) Mean ages and (b) modal times characteristic of the age spectra which best reproduce the CO_2 observations at 420 K (green circles), 440 K (red triangles), and 460 K (blue diamonds). The lines are the result of a nonlinear least squares regression versus time and potential temperature for the profiles on 14 equally spaced isentropes from 395 to 460 K (see text for details). The results for December 1996 were not included in the fit because of the anomalously low modal times obtained for this flight. Error bars reflect only the range of solutions obtained from the Monte Carlo analysis and do not include uncertainty in the CO_2 boundary condition or in the assumption of a functional form for the Green's function. (**c**) The age spectra at 420 K (green), 440 K (red), and 460 K (blue) corresponding to the date with the predicted maximum (September 15) and (**d**) minimum (March 15) mean age at 460 K.

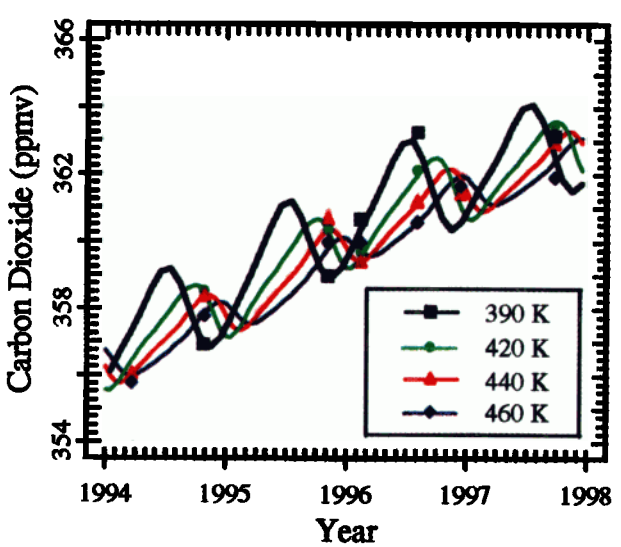

Plate 2. Evolution of CO_2 as a function of time and potential temperature from convolution of the boundary condition from Figure 2 with age spectra generated from the fits to the Γ and τ_M shown in Plates 1a and 1b. The black line labeled 390 K is the stratospheric boundary condition. Symbols represent the median of the observations within 1 K of the isentrope for each of the CO_2 profiles shown in Figure 1.

Table 1. Coefficients for Equation (5), Variation of Γ and τ_M With Time of Year and Potential Temperature

	Γ	τ_M
a_1 (yr/K)	6.41×10^{-3}	3.45×10^{-3}
a_2 (yr/K^2)	8.51×10^{-6}	1.68×10^{-5}
a_3 (yr/K)	2.83×10^{-3}	2.08×10^{-3}
a_4 (yr/K$^{2)}$	-2.39×10^{-5}	-1.80×10^{-5}
a_5 (K^{-1})	-1.69×10^{-3}	-2.28×10^{-3}
a_6	0.645	0.623

to the proximity of the flight to the time of occurrence of the seasonal minimum. An obvious extratropical filament below 425 K (visible in Figure 1) further complicates the interpretation. This flight is therefore given low weight in our analysis.

5. Results and Discussion

5.1. Γ, τ_M, and Δ from the Empirical Age Spectra

Our method provides accurate mean ages for the lower tropical stratosphere, which are difficult to obtain by simple analysis of lag times from tracer measurements. For example, the SF_6 boundary condition at the tropical tropopause is not so well known as that for CO_2, and the persistence of the seasonal cycle causes ambiguity in lag times derived from CO_2. These factors are significant sources of error for air with $\Gamma < 1$ year.

The mean ages in Plate 1a are 30-40% younger in NH winter than during the rest of the year. Seasonal variations in τ_M are also apparent (Plate 1b), although the amplitude is smaller than for Γ. To examine the propagation of variations in CO_2 and other tracers using seasonally varying age spectra, it is convenient to have a spatially and temporally continuous representation of Γ and τ_M. The lines in Plates 1a and 1b represent fits obtained by a nonlinear least squares regression of the optimum mean ages and modal times for six time periods on 14 evenly spaced isentropes from 395 to 460 K using the functional form

$$\Gamma(\text{or } \tau_M) = a_1\theta + a_2\theta^2 + (a_3\theta + a_4\theta^2)\sin(\omega(t + a_5\theta + a_6)) \quad (5)$$

where $\omega \equiv 2\pi/(1 \text{ year})$ and t is time in years (results for December 1996 were not included in the regression because of the sensitivity to the boundary condition discussed above). The CO_2 profiles corresponding to this regression, i.e., the predicted profiles from the seasonally varying age spectra, are shown as dotted lines in Figures 1a-g and the values of the coefficients a_i are given in Table 1. For comparison, the dashed lines in Figure 1 were generated using annually averaged values of Γ and τ_M. Solutions are better constrained for altitudes with potential temperatures < 440 K than for higher altitudes because the available CO_2 profiles do not contain identifiable extrema between 440 and 460 K.

Comparison of the CO_2 profiles calculated from the seasonally varying versus annually averaged age spectra shows that the changes in CO_2 mixing ratio associated with the seasonal oscillations in Γ and τ_M are relatively small but large enough to be detected. Given our imperfect knowledge of the CO_2 boundary condition, however, it is unclear how accurately we can determine such small differences in Γ and τ_M, although they appear to be reproducible and statistically significant for this set of observations. Younger mean ages in NH spring are consistent with faster ascent rates during NH winter, as predicted by the concept of the "extratropical wave-driven pump" [*Holton* et al., 1995]. We relate our results to a seasonally varying 1-D model of atmospheric transport in the discussion below and show that the seasonal changes in the derived vertical velocity agree well with those determined from seasonally resolved radiative calculations [*Rosenlof*, 1995; *Eluszkiewicz et al.*, 1996].

The age spectra for 420, 440, and 460 K are illustrated in Plates 1c and 1d for the dates with predicted minimum (March 15) and maximum (September 15) mean ages at

Table 2. Phase Lag Times and Attenuation for CO_2, CO_2^{seas}, and $CO_2^{2\pi/yr}$

		Date of Seasonal Extremum		Phase Lag Time (days)		Peak-to-Peak Amplitude (ppmv)*	Fraction of Amplitude Remaining	Percent of Attenuation Due to Erosion of Each Extremum	
		MAX	MIN	MAX	MIN			MAX	MIN
CO_2									
	390	July 1	Nov. 15	-	-	3.21	1.00	-	-
	420	Oct. 1	Jan. 15	91	53	2.29	0.71	62	38
	440	Nov. 7	Feb. 15	128	91	1.69	0.53	50	50
	460	Dec. 15	March 15	166	122	1.26	0.39	48	52
CO_2^{seas}									
	390	July 1	Nov. 15	-	-	3.21	1.00	-	-
	420	Sept. 15	Jan. 15	75	61	2.45	0.76	64	36
	440	Nov. 1	March 1	122	108	1.88	0.58	57	43
	460	Dec. 1	April 1	152	138	1.42	0.44	54	46
$CO_2^{2\pi/yr}$									
	390	June 15	Dec. 15	-	-	2.97	1.00	-	-
	420	Sept. 1	Feb. 1	77	47	2.36	0.79	71	19
	440	Oct. 15	March 1	122	77	1.85	0.62	62	38
	460	Dec. 1	April 1	168	108	1.40	0.47	54	46

*To obtain an estimate of the peak-to-peak amplitude for CO_2, we neglected interannual variation in the growth rate and subtracted a line with a slope of 1.5 ppmv/yr from the signal on each isentrope, leaving the variation associated with the propagation of CO_2^{seas} as well as the induced oscillation due to seasonally varying transport rates (see discussion of Figure 3a).

460 K. The September spectrum at 460 K is somewhat wider (Δ = 0.22 years) than the March spectrum (Δ = 0.16 years). We note that the ratio of spectral width to mean age is relatively constant throughout the year, ranging from Δ/Γ=0.35 in January to Δ/Γ = 0.42 in July at 460 K. The variation in Δ/Γ at lower altitudes is slightly larger, from 0.35 in early December to 0.51 in early March at 420 K.

The attenuation of the CO_2 seasonal cycle is very sensitive to Δ, which measures the relative roles of advective and diffusive processes. For purely advective transport, the age spectrum would resemble a delta function, and no attenuation of the seasonal cycle would occur. Our results indicate that the CO_2 seasonal cycle at 460 K is reduced to approximately half its amplitude at the tropical tropopause (see Table 2 and discussion below).

Plate 2 shows the CO_2 time series at 420, 440, and 460 K computed by convolution of the seasonally varying age spectra with the stratospheric boundary condition. The symbols represent the median of the observations within ±1 K of the isentrope for each of the profiles in Figure 1. In November 1995 the predicted maximum occurs at a lower potential temperature and is more attenuated than observed. In December 1996 the predicted values are higher than those observed at both 440 and 460 K. From the individual profiles in Figure 1, the nature and significance of these discrepancies are not obvious. However, when examined in the context of the entire time series, it is evident that the differences between the predicted and the observed profiles can be explained by slight shifts in the phase or amplitude of the boundary condition or by small interannual differences in transport rates.

These derived values of Γ, τ_M, and Δ should serve as powerful diagnostics for transport parameterizations in stratospheric models. Unfortunately, most currently available age spectra from models have been computed with respect to the surface rather than the tropical tropopause. Errors associated with removing the tropospheric component from existing model age spectra are likely to be of the same magnitude as the derived values for Γ, τ_M, and Δ in the lower tropical stratosphere. Also, studies of model age spectra have not allowed for seasonal variation in transport rates. Thus it is not useful at present to compare our results to published age spectra from models.

A rigorous estimate of the uncertainty in the derived age spectra is difficult to obtain because systematic errors dominate, including imperfect knowledge of the CO_2 boundary condition and possible interannual variations in transport rates. The seasonality in the derived age spectra is strongly influenced by the data from a single month (February 1996) due to ambiguities in the solutions for March 1994 and December 1996 discussed above. It is harder to quantify the systematic error associated with our assumption that transport in the lower tropical stratosphere can be adequately represented using the functional form for the Green's function derived from a solution to the 1-D diffusion equation.

The sensitivity of the values for Γ and τ_M to uncertainty in the boundary condition was tested by introducing small perturbations in its amplitude and phase and repeating our analysis. Seven cases were tested, covering the range of uncertainty in the boundary condition. The optimum mean ages and modal times obtained using the perturbed boundary conditions were generally within ± 0.05 years of those reported above, but the quality of the corresponding fits to the CO_2 profiles was diminished. The October 1994 and November 1995 profiles were obtained within 2 weeks of each other but in different years. The values of Γ and τ_M for these flights are quite similar (see Plate 1), demonstrating that our results are reproducible for this time of year. Finally, our ability to reproduce observed H_2O profiles (see below) using the empirical age spectra provides independent evidence of the validity of the method and results. Additional tropical CO_2 profiles, particularly for times between December and July, would help verify the seasonality in the derived age spectra and provide insight into interannual variability in transport rates.

5.2. Phase Lag Times and Attenuation for CO_2 Seasonal Extrema

Phase lag times and attenuation rates have been derived from observations of propagating seasonal extrema in CO_2 [Boering et al, 1996] and H_2O [*e.g.*, Mote et al., 1996, 1998] mixing ratios. These quantities are sensitive to the rates for advection and diffusion in the stratosphere and are therefore powerful diagnostics of transport parameterizations in numerical models.

To obtain a more complete understanding of the spatial and temporal evolution of the propagating CO_2 signal, it is helpful to separately consider the propagation of its fundamental components. The CO_2 boundary condition can be written as

$$CO_2 = CO_2^{trend} + CO_2^{seas},$$

where CO_2^{trend} is the long-term positive trend and CO_2^{seas} is the seasonal oscillation. To simplify the following discussion, we neglect interannual variation in the CO_2 growth rate, so CO_2^{trend} increases linearly at a constant rate of 1.5 ppmv/yr. CO_2^{seas} can be further decomposed into annual and semiannual Fourier harmonics with frequencies of 2π/yr and 4π/yr, respectively,

$$CO_2^{seas} = CO_2^{2\pi/yr} + CO_2^{4\pi/yr}.$$

Using the derived age spectra, equation (1) can be applied to the individual components of the boundary condition to produce time series on various isentropes that show the propagation of each component. Estimates of the attenuation and phase lag times for CO_2, CO_2^{seas}, and $CO_2^{2\pi/yr}$ are summarized in Table 2 and discussed in detail below. Note that the peak-to-peak amplitude of an oscillating tracer can be diminished by erosion of either the maximum or the minimum or both. We therefore include the percentage of attenuation associated with each extremum, relative to the peak-to-peak amplitude at 390 K, in columns 8 and 9 of Table 2.

Consider first the propagation of CO_2^{trend}. Seasonal variations in transport rates distort the signal, inducing a seasonal oscillation on an isentrope, superposed on the positive trend (Figure 3a). In NH spring, when mean ages reach a minimum, tracer mixing ratios are higher than they would be in the absence of seasonally varying transport, and conversely for autumn. The phase of the induced seasonal oscillation in CO_2^{trend} is nearly opposite to the phase of CO_2^{seas} (compare Figure 3b). This phase interference reduces the apparent amplitude of the CO_2 seasonal cycle by 12% at 460 K (compare attenuation of CO_2 with that of CO_2^{seas} in Table 2). If the magnitude of seasonal variations in transport rates has been underestimated, this effect would be larger. This mechanism attenuates the CO_2 seasonal cycle more rapidly than the seasonal cycle of another tracer that does not have a significant long-term trend (e.g., H_2O).

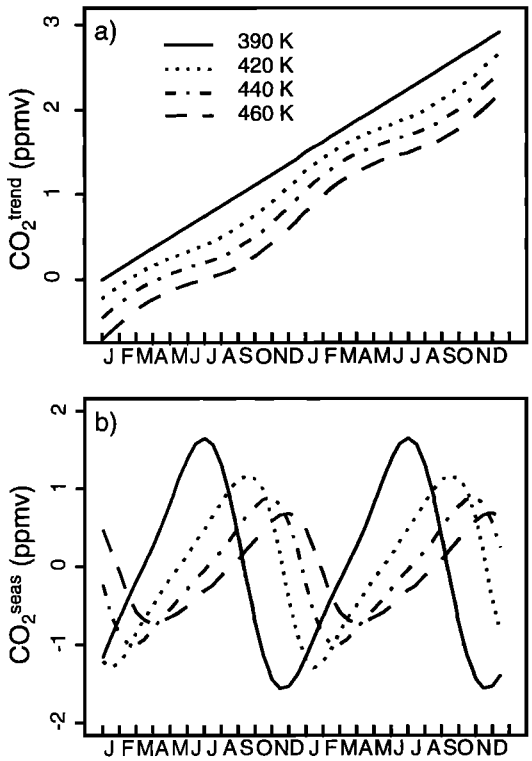

Figure 3. (a) Evolution with increasing potential temperature and time of CO_2^{trend}, a linearly increasing tracer with a slope of 1.5 ppmv/yr (the long-term average growth rate of CO_2), and (b) CO_2^{seas}, the two-harmonic representation of the seasonally varying component of the CO_2 signal. A constant offset has been applied to the values in (a) so that the initial value of CO_2^{trend} is 0 ppmv at 390 K. Two years are shown for clarity.

Mixing of older, extratropical air into the tropical upwelling region decreases the mean value of the propagating CO_2 signal because of the long-term increase in CO_2. This distortion of the CO_2 profile causes vertically propagating seasonal minima (maxima) to appear at higher (lower) altitudes than if there were no mixing with extratropical air. *Hall and Waugh* [1997b] identified this distortion as a potential source of error in diagnosing ascent rates based on the phase lag times for CO_2 seasonal extrema, as in the work of Boering *et al.* [1996]. Comparison of profiles of CO_2 and CO_2^{seas} (not shown) indicates that between 420 and 460 K, shifts of 5 - 10 K in the location of the extrema are likely, which correspond to changes in the phase lag times of 5 to 20 % (see Table 2). These changes in the calculated phase lag times are relatively small, reflecting the narrow widths ($\Delta < 0.5\ \Gamma$) of the empirical age spectra. However, phase lag times for propagating minima are longer for CO_2^{seas} than for the overall CO_2 signal, while those for maxima are shorter, so that ascent rates inferred from CO_2^{seas} would have significantly less seasonality than those inferred directly from CO_2 observations. Note that complications associated with the fact that CO_2^{seas} includes both annual and semiannual harmonics also affect the phase lag times and must be taken into account, as discussed below.

The separate and aggregate evolution of $CO_2^{2\pi/yr}$ and $CO_2^{4\pi/yr}$ are shown in Figure 4. As these signals propagate into the stratosphere, the higher-frequency component is attenuated much more rapidly than the annually varying component, because of its shorter vertical wavelength [*Hall and Waugh*, 1997a]. The semiannual mode is nearly completely attenuated by the time the signal reaches 460 K. This rapid attenuation of the higher-frequency component can affect estimates of attenuation and phase lag times depending on the nature of the interference between the harmonics at the lower boundary (i.e., whether the extrema interfere constructively or destructively and whether the times for the extrema are advanced or delayed). For example, $CO_2^{2\pi/yr}$ is slightly less attenuated than CO_2^{seas} at 460 K since CO_2^{seas} has a larger amplitude at 390 K, resulting from constructive interference of $CO_2^{2\pi/yr}$ and $CO_2^{4\pi/yr}$. Also, the phase lag time for the minimum in CO_2^{seas} at 460 K is roughly 25% longer than that of $CO_2^{2\pi/yr}$, while the phase lag time for the maximum is about 10% shorter.

Consideration of the purely annual cycle, $CO_2^{2\pi/yr}$, allows the effects of seasonal variations in transport rates to be isolated from distortion of the CO_2 signal associated with the selective attenuation of $CO_2^{4\pi/yr}$ and the propagation of CO_2^{trend}. Broader age spectra in NH summer cause the seasonal maximum to be slightly more attenuated than the minimum. This differential attenuation is most pronounced between 390 K and 420 K. The maximum in $CO_2^{2\pi/yr}$ travels through this region from June 15 to September 1, while the minimum propagates from December 15 to February 1 when the age spectra are narrowest. Phase lag times are similarly affected, with the phase lag time for the minimum 40 to 50% shorter than that for the maximum over the altitude range considered. Accordingly, ascent rates estimated from the phase lag times for $CO_2^{2\pi/yr}$ are ~45% greater for the mini-

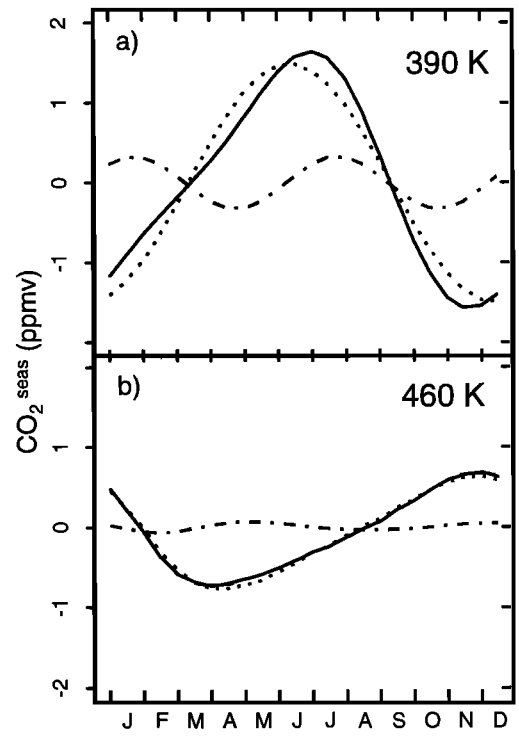

Figure 4. Annual ($CO_2^{2\pi/yr}$, dotted curves) and semiannual ($CO_2^{4\pi/yr}$, dotted-dashed curves) harmonics of the CO_2 seasonal cycle and their sum (CO_2^{seas}, solid curves) at (a) 390 K and (b) 460 K showing the relatively greater attenuation of the semiannual harmonic over this height range.

mum than for the maximum at 440 K. This value is quite similar to the 38% derived directly from observed CO_2 profiles by *Boering et al.* [1996] because the effects of the long-term trend and the rapid attenuation of $CO_2^{4\pi/yr}$ largely cancel.

Hall and Plumb [1994] and *Hall and Waugh* [1997b] discussed the relationships among Γ, τ_M, and τ_ω, the phase lag time for a sinusoidally varying tracer with frequency ω. In the 1-D diffusion case, Γ and τ_ω are approximately equal when $\Delta^2/\Gamma << 1/\omega$ [*Hall and Plumb*, 1994]. The derived age spectra approximately satisfy this condition throughout the year ($\Delta^2/\Gamma \cong$ 0.02-0.09 years between 400 and 460 K), with the largest differences between Γ and τ_ω for sinusoidal extrema entering the stratosphere in March and April and propagating through the stratosphere during NH spring and summer (τ_ω/Γ = 0.6 - 0.7). The phase lag times for the extrema of $CO_2^{2\pi/yr}$ range from 70 to 90% of the values for Γ at the corresponding potential temperature and time (compare phase lag times from Table 2 with Γ from Plate 1a). *Hall and Waugh* [1997b] noted similarity between τ_M and τ_ω in 3-D model results for the tropics. We find that $\tau_M < \tau_\omega$ throughout the potential temperature range considered, with τ_M/τ_ω ranging from 0.6 to 0.9 from 420 to 460 K. The smallest differences between τ_M and τ_ω occur at the highest potential temperatures and show no significant seasonality.

5.3. Analysis of Water Vapor using Empirical Age Spectra

Observations of stratospheric H_2O have been used for diagnosing stratospheric transport since the 1940s [*Brewer*, 1949]. Recently, *Dessler* [1998] calculated H_2O saturation mixing ratios for the minimum temperature in each of the (~60,000) radiosonde profiles obtained between 10°S and 10°N from 1994 to 1997 and showed that the annual averages of these mixing ratios are consistent with observed humidity in the lower stratosphere. This view represents a departure from previous analyses, which concluded that mean tropical tropopause temperatures are too warm to account for the observed dehydration of the stratosphere [e.g., *Newell and Gould-Stewart*, 1981], prompting speculation that air must preferentially enter the stratosphere through regions with locally colder tropopause temperatures.

Monthly mean saturation mixing ratios for the tropical tropopause region from 1993 to 1997 have been similarly calculated from the radiosonde temperature profiles (A. E. Dessler, personal communication, 1998). The resulting time series exhibits a seasonal oscillation with an amplitude of approximately 2.8 ppmv (Figure 5). Another recent analysis (E. M. Weinstock et al., Evaluation of the seasonal cycle of water vapor in the stratosphere derived from monthly average tropical tropopause temperatures using a CO photochemical clock, submitted to *J. Geophys. Res.*, 1999) showed that in situ measurements of tropical H_2O from the ER-2 during STRAT are consistent with this monthly mean water vapor boundary condition. Satellite observations also show a seasonal oscillation in H_2O mixing ratios entering the stratosphere but with a much smaller amplitude [e.g., *Randel et al.*, 1998, *Mote et al.*, 1996, 1998]. Accurate knowledge of the stratospheric boundary condition for H_2O would strongly constrain proposed mechanisms for troposphere-to-stratosphere transport and would reduce the uncertainty in studies of transport within the stratosphere based on the propagation and attenuation of the H_2O seasonal cycle. The empirical age spectra enable us to further investigate whether the in situ observations are consistent with the boundary condition proposed by Dessler and Weinstock et al.

We used a smoothed representation of the monthly mean H_2O saturation mixing ratios as the stratospheric boundary condition (Figure 5, solid curve) and convolved that with our empirical age spectra to generate the vertical H_2O profiles shown in Figure 6 (solid curves). H_2O produced in the stratosphere by CH_4 oxidation has been subtracted from the data in Figure 6 using observed CH_4 and assuming that two molecules of H_2O are produced per molecule of CH_4 oxidized [*Dessler et al.*, 1994; *Hurst et al.*, 1999]. The correction is small (< 0.2 ppmv) for the data considered here.

The profiles generated from the age spectra clearly capture many detailed features of the observations. However, the data for August and December 1996 do not support the lower mixing ratios for the seasonal maximum in 1996 indicated by the proposed boundary condition. In fact, the in situ data for both August and December 1996 contain mixing ratios exceeding the seasonal maximum in the proposed boundary condition for that year, which is lower than those for the other four years by more than 1 ppmv (~30 %). To examine the sensitivity of our calculated profiles to this feature, we determined an average seasonal cycle for 1993-1997 by fitting a function with annual and semiannual harmonics to the monthly mean H_2O mixing ratios (dashed curve in Figure 5).

Agreement between the data and the profiles computed using this two-harmonic fit to the boundary values (dashed curves in Figure 6) is markedly improved for December 1996, although not noticeably improved for August 1996. Given the large uncertainty associated with the tropical tropopause-region saturation mixing ratios (20%) and the temporal and spatial resolution of the in situ data used in this analysis, especially the limited longitudinal coverage of the profiles (150°-175°W), we are unwilling to speculate whether this improved agreement for December 1996 reflects a problem with the proposed H_2O boundary condition for that year or real interannual variability in either the boundary condition or the transport within the lower tropical stratosphere. Recall that the values for Γ and τ_M obtained from the CO_2 data for December 1996 were also anomalous, further complicating the analysis for that flight.

Despite the uncertainty associated with the December 1996 data, the overall agreement between the observations and the calculated profiles provides significant evidence that on average the seasonal cycle defined by the monthly mean saturation mixing ratios closely approximates the true stratospheric boundary condition for water vapor.

Peak-to-peak amplitudes from the extended empirical orthogonal function (EEOF) analysis of *Mote et al.* [1998] and the harmonic analysis of *Randel et al.* [1998] of observations of $H_2O + 2*CH_4$ from the Halogen Occultation Experiment (HALOE) are shown in Figure 7 along with those obtained from the age spectra using the two-harmonic boundary condition for H_2O. These quantities are directly comparable since H_2O is conserved in the age spectrum analysis.

Our results suggest that satellite-borne instruments underestimate the amplitude of the seasonal cycle near the tropopause, possibly because of insufficient vertical resolution combined with the short vertical wavelength of the propagating tracer signal in this region. To compare attenuation from different studies, amplitude is frequently normalized to the

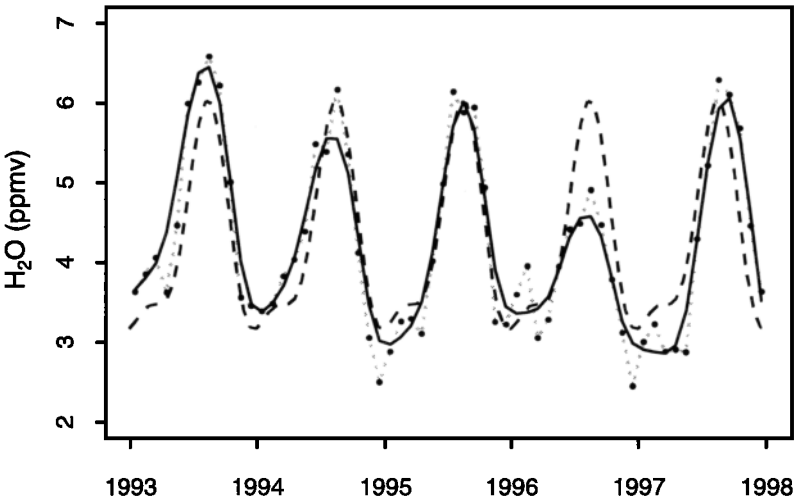

Figure 5. Time series of H_2O saturation mixing ratios at the tropical tropopause (A. E. Dessler, personal communication, 1998). Each point represents the monthly mean of saturation mixing ratios determined from ~1250 radiosonde temperature and pressure profiles from 10°S to 10°N as in the work of *Dessler* [1998]. The estimated uncertainty in the values is 20%. The solid curve is a smoothed representation of the monthly mean mixing ratios and the dashed curve is a fit with annual and semiannual harmonics.

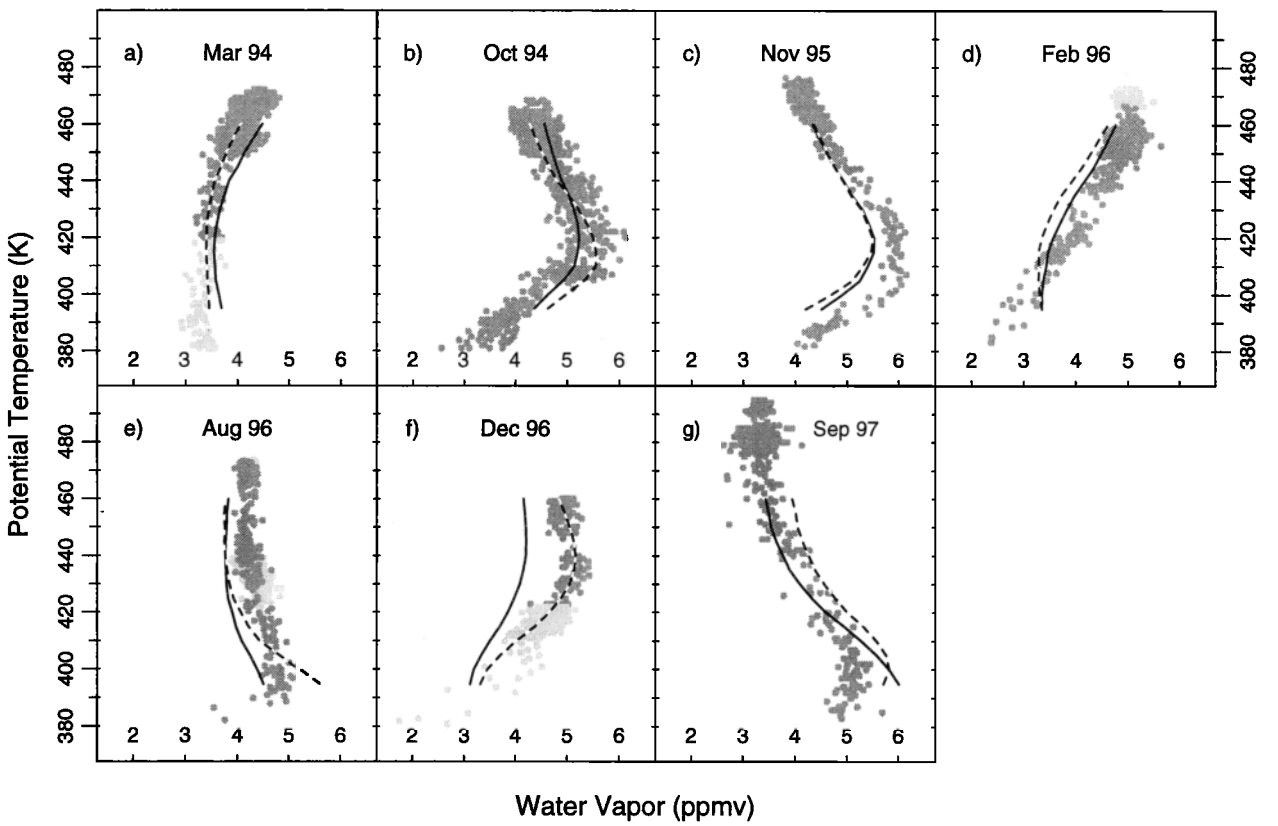

Figure 6. H_2O observations corrected for CH_4 oxidation (symbols; see text) and profiles generated by convolving the empirical age spectra with the smoothed representation of the boundary condition shown in Figure 5 (solid curves) and with the two-harmonic fit to the monthly mean H_2O mixing ratios for 1993-1997 (dashed curves). Data for March and October 1994 were obtained using the NOAA Lyman-α instrument [*Kley et al.*, 1983] during ASHOE/MAESA. The remaining profiles were obtained using the Harvard University Lyman-α instrument during STRAT and POLARIS [*Weinstock et al.*, 1994]. Shading of the points is the same as in Figure 1.

tropopause value so that the amplitude ranges from 0 to 1. Normalizing the results in Figure 7 to the 390 K values indicates reasonably good agreement over the altitude range considered here. However, the implicit assumption when normalizing in this manner is that any bias in a particular set of observations or results is constant with altitude, and more in situ data for potential temperatures > 460 K is needed to demonstrate unambiguously that there is no significant altitude variation in HALOE's ability to resolve the seasonal cycle in $H_2O + 2*CH_4$.

Such validation is required for reliable analysis of tracer data from satellites. For example, if HALOE is able to resolve a larger fraction of the seasonal amplitude at higher altitudes than near the tropopause, studies based on HALOE data alone will underestimate the role of diffusive processes which attenuate propagating tracer signals in the lowest several kilometers of the stratosphere. This may represent an explanation for the extremely long timescales for mixing of air from higher latitudes into the tropics reported by *Mote et al.* [1998] between 20 and 24 km computed using HALOE observations of $H_2O + 2*CH_4$. They obtain timescales from 40 to 80 months for this region, while *Minschwaner et al.* [1996] and *Herman et al.* [1998] find significantly shorter timescales of 8-20 and 8-44 months, respectively, using balloon observations of N_2O and other tracers. Note that both *Minschwaner et al.* [1996] and *Herman et al.* [1998] neglect vertical diffusion, which is generally assumed to be small in the tropics. However, vertical diffusion is included in the study by *Mote et al.* [1998] and could potentially account for some of the discrepancy.

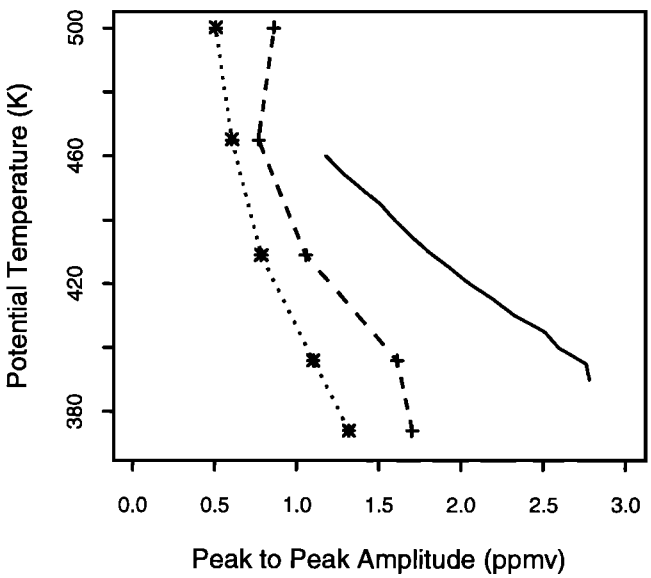

Figure 7. Peak-to-peak amplitude of the seasonal cycle in H_2O as predicted using the empirical age spectra with the two-harmonic fit to the monthly mean saturation mixing ratios (solid line). Peak-to-peak amplitudes of $H_2O + 2*CH_4$ from the extended empirical orthogonal function (EEOF) analysis of *Mote et al.* [1998] (dotted line with asterisks) and the harmonic analysis of *Randel et al.* [1998] (dashed line with crosses) are shown for comparison. An average relationship from ER-2 and balloon data was used to relate pressure and potential temperature.

5.4. Estimates of Q and K_θ

To understand how our results compare to previous studies and to illustrate how they constrain proposed transport mechanisms, it is useful to consider a simple 1-D advection-diffusion model of transport

$$\rho\frac{\partial n(\theta,t)}{\partial t}=\frac{\partial}{\partial\theta}\left(K_\theta\rho\frac{\partial n(\theta,t)}{\partial\theta}\right)-\rho Q\frac{\partial n(\theta,t)}{\partial\theta} \quad (6)$$

where θ is the potential temperature above the tropopause, ρ is the air density, Q is the diabatic heating rate (ascent rate in isentropic coordinates), and K_θ is a diffusion coefficient. For constant Q and K_θ, the associated Green's function is given by

$$G(t,\theta;\theta_o)=\frac{\theta}{2\sqrt{\pi K_\theta t^3}}\exp\left(\left(\frac{\theta}{2H_\theta'}\right)-\left(\frac{K_\theta}{4H_\theta'^2}\right)t-\frac{\theta^2}{4K_\theta t}\right) \quad (7)$$

where

$$H_\theta'=H_\theta\left(1+\frac{QH_\theta}{K_\theta}\right)^{-1},$$

and H_θ is the scale height (equation (21) from *Hall and Plumb* [1994] written in isentropic coordinates and modified to include advection). We use $H_\theta = 150$ K, corresponding to $H_z = 6$ km from the mean observed temperature for the tropical profiles, 200 ± 3 K, and the observed relationship between potential temperature and altitude, $\partial\theta/\partial z = 25$ K/km.

We can use the above equation to obtain estimates of $\bar{Q}$ and $\bar{K}_\theta$ from our coefficients B and C,

$$\bar{K}_\theta=\frac{\theta^2}{4C} \quad (8a)$$

$$\bar{Q}=-\frac{\theta^2}{4H_\theta C}+\theta\sqrt{\frac{B}{C}}. \quad (8b)$$

Estimates for $\bar{K}_\theta$ and $\bar{Q}$ as a function of time of year are shown in Figures 8a and 8b for the seasonally varying age spectra. These values correspond to $\Gamma(\theta, t)$ and $\tau_M(\theta, t)$ given by equation (5), and the overbar is intended to emphasize that they represent average values from the tropopause to θ, rather than instantaneous values for a particular θ and time. This averaging is responsible in part for the decreasing seasonal variation with increasing potential temperature.

The slope of potential temperature versus altitude ranges from 20 K/km in February 1996 to 28 K/km in October 1994 and November 1995. Intermediate values are found for the other profiles, with lower values in December to March than in August to November. This seasonal variation in $\partial\theta/\partial z$ has a negligible effect on our derived values of Q (≤ 2%) and no effect on K_θ. However, there is an effect on estimates of the ascent rate w and diffusion coefficient K_z expressed in altitude coordinates, which are included in Figure 8 to facilitate comparison of our results with those from previous studies. In altitude coordinates the effect of the seasonality in $\partial\theta/\partial z$ is amplified, so w and K_z could be as much as 25% and 56% larger, respectively, from December to March and 15% and 30% smaller, respectively, from August to November.

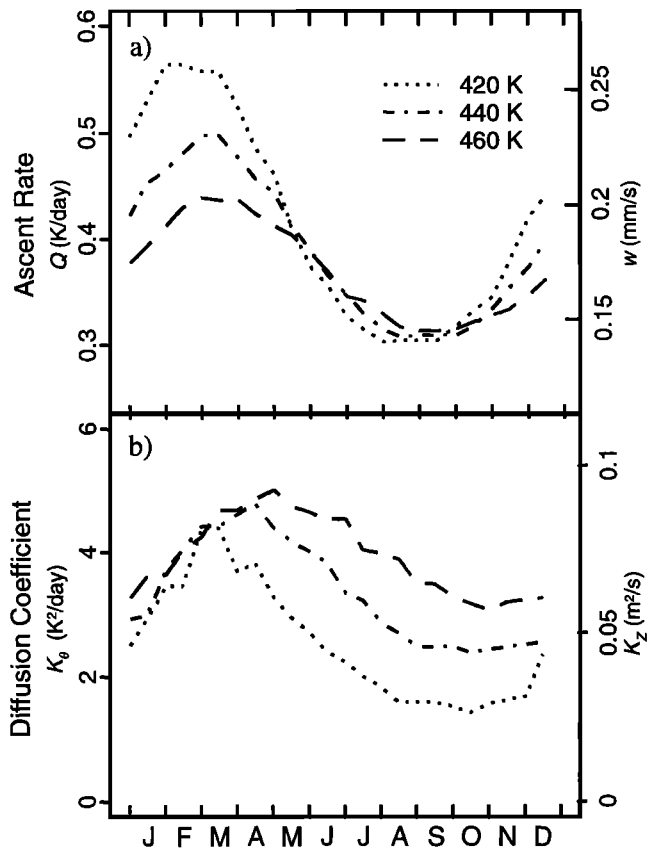

Figure 8. Seasonal variation of vertical velocity Q (a) and the effective vertical diffusion coefficient K_θ (b) derived from the empirical age spectra at 420, 440, and 460 K. K_θ includes both vertical and quasi-horizontal isentropic diffusion and thus represents an upper limit on the true vertical diffusion coefficient. The scales in altitude coordinates (mm/s and m^2/s) on the right axes are subject to large uncertainty associated with seasonal variation in $\partial\theta/\partial z$ (see text).

The calculated ascent rates are larger in NH winter, as expected from the extratropical wave-driven pump theory [*Holton et al.*, 1995], and are notably consistent with seasonally resolved vertical velocities calculated from radiative heating rates and satellite and climatological data. *Rosenlof* [1995] reported ascent rates for the equatorial region of 0.4 and 0.1 mm/s, respectively, in January and July 1993 at 70 mbar (~ 18.5 km). *Eluszkiewicz et al.* [1996] found values of 0.23 mm/s for July through October and 0.3 mm/s for November through February averaged from 15°S to 15°N between the tropopause and 21 km. Comparison of values for Q with ascent rates based on the propagation of seasonal extrema in CO_2 [*Boering et al.*, 1996] indicates close agreement, as discussed above. Our results are also consistent with ascent rates from studies based on HALOE observations of H_2O + 2*CH_4. For example, *Mote et al.* [1996] reported values of 0.4 mm/s during NH winter and 0.2 mm/s for the rest of the year, based on the propagation of the seasonal extrema. Two subsequent studies of HALOE H_2O + 2*CH_4 used a simple 1-D model, which included a representation of mixing of extratropical air into the tropical upwelling region, and obtained annual mean vertical velocities for the lower tropical stratosphere of 0.20 - 0.35 mm/s [*Mote et al.*, 1998] and 0.5 K/day (~0.3 mm/s) [*Hall and Waugh*, 1997b].

The values for $\bar{K}_\theta$ include contributions from both vertical diffusion and quasi-horizontal mixing with air from higher latitudes. They therefore represent an upper limit on the vertical diffusion coefficient and are generally consistent with those calculated in other recent studies in cases where the timescale for mixing of air from midlatitudes into the tropical upwelling region (τ_{IN}) was set to be infinitely long. For example, *Mote et al.* [1996] derived 0.03-0.09 m^2/s and *Hall and Waugh* [1997b] obtained 1.8 K^2/day (~0.04 m^2/s) for this limit.

Because the 1-D advection-diffusion model does not explicitly include mixing of extratropical air into the tropics, all of the broadening of the age spectrum is attributed to diffusion in this analysis. Isentropic mixing with extratropical air can only increase the mean age of an air parcel, but the effect of diffusion on mean age is somewhat ambiguous. At a particular altitude, diffusion of air from above would increase the mean age, while diffusion of air from below would tend to make the air parcel younger. The impact of diffusion on the mean age is therefore determined by $\partial K_\theta/\partial\theta$ and $\partial\Gamma/\partial\theta$.

Our estimates of $\bar{K}_\theta$ and $\bar{Q}$ indicate that the timescale for diffusion is much longer than that for advective ascent, so vertical diffusion has little effect on the mean age. In fact, the mean age is nearly indistinguishable from the ascent timescale ($\Gamma \cong \Delta\theta/Q$) in this analysis. In the atmosphere, mixing with old air from the extratropics could also increase the age of an ascending air parcel. Therefore our values of $\bar{Q}$ probably represent a lower limit on the vertical velocity. The ascent rates presented here are indeed somewhat smaller than those reported by *Mote et al.* [1998] and *Hall and Waugh* [1997b], which were derived using a 1-D model that includes a parameterization of mixing of air from higher latitudes into the tropics. The fact that we do not obtain greater differences from their results probably reflects the relative dominance of advective processes in this region of the atmosphere. However, this comparison is not completely straightforward because those studies were based on HALOE observations of H_2O + 2*CH_4 and may therefore underestimate the attenuation of the seasonal cycle near the tropopause, as discussed in conjunction with Figure 7.

Because of the inherent uncertainty in assuming that transport in the lower tropical stratosphere can be adequately represented by such a simple model, it is not possible to quantitatively estimate the error in the calculated values of $\bar{Q}$ and $\bar{K}_\theta$. However, the fact that our results are generally consistent with independent estimates of these parameters increases our confidence in the empirical age spectra and suggests that the 1-D advection-diffusion model captures the essential characteristics of transport in this region. In addition, although the apparent seasonality in the age spectra is comparable to the level of uncertainty in this analysis (see Plate 1 and the associated discussion), it is consistent with the current understanding of the dynamics driving upwelling in the tropics, and the agreement between our estimated vertical velocities and those from radiative transfer calculations provides additional evidence that this seasonality is real.

6. Conclusions

We have shown that empirical age spectra for the lower tropical stratosphere can be obtained from our time series of observations of CO_2 mixing ratios. The derived age spectra represent a complete description of transport from the lower

boundary into the first several kilometers of the lower tropical stratosphere. Our method provides accurate mean ages for this region, where analyses of lag times from tracer measurements are subject to large uncertainties.

Age spectra provide powerful tools for detailed analyses of tracer data, providing new insight into the mechanisms controlling the propagation and attenuation of the CO_2 and H_2O seasonal cycles and into transport rates of trace species in the lower tropical stratosphere. We have shown that propagating tracer signals can be significantly distorted by seasonal variations in transport rates and, in the case of seasonally varying tracers, by selective attenuation of higher-frequency components.

Our results provide stringent tests of model transport in a form that is directly comparable to model outputs. Models and observations must both have sufficient resolution to accurately resolve propagating tracer signals, which have a vertical scale of ~1 km. Currently, models and satellite observations are both limited in this respect. Relatively small variations in mean age, modal time, and spectral widths can have significant implications for tracer transport.

Transport in the lower tropical stratosphere is primarily advective, as recognized since the days of Brewer and Dobson, but velocities are small, allowing relatively weak diffusive processes to significantly attenuate periodic signals. Thus even small rates for diffusion may be important in regulating tracer distributions. The relative rates of advection and diffusive processes must therefore be accurately represented in model simulations of stratospheric chemistry.

Acknowledgments. We thank K. K. Kelly for use of the H_2O data from ASHOE/MAESA; T. M. Hall, D. W. Waugh, R. A. Plumb; and two anonymous reviewers for helpful comments on the manuscript; L. Kogan for many stimulating discussions; W. J. Randel and P. W. Mote for providing HALOE observations and analysis results; T. J. Conway for surface CO_2 data from the NOAA, CMDL carbon cycle group; A. E. Dessler for providing monthly mean H_2O saturation mixing ratios; C. R. Webster's group for CH_4 data; M. Loewenstein's group for N_2O data; J. W. Elkins' group for CFC data; M. Proffitt's group for O_3 data; D. W. Fahey's group for NO_y data; B. L. Gary's group for tropopause heights; and S. Alex, A. Bazzaz, and J. Lipson for field support. We are grateful for the efforts of all the ER-2 investigators, coordinators, pilots, and crew. This research was supported by the NASA Upper Atmospheric Research Program and Atmospheric Effects of Aviation Project, by NASA grants NCC2-694 (CO_2), and NCC2-913 (H_2O) to Harvard University. KAB was supported in part by a U.S. Department of Energy Global Change Distinguished Postdoctoral Fellowship and a Bunting Institute of Radcliffe College Science Scholars Fellowship.

References

Avallone, L. M., and M. J. Prather, Photochemical evolution of ozone in the lower tropical stratosphere, *J. Geophys. Res.*, *101*, 1457-1461, 1996.

Bischof, W., R. Borchers, P. Fabian, and B. C. Krüger, Increased concentration and vertical distribution of carbon dioxide in the stratosphere, *Nature*, *316*, 708-710, 1985.

Boering, K. A., B. C. Daube, S. C. Wofsy, M. Loewenstein, J. R. Podolske, and E. R. Keim, Tracer-tracer relationships and lower stratospheric dynamics: CO_2 and N_2O correlations during SPADE, *Geophys. Res. Lett.*, *21*, 2567-2570, 1994.

Boering, K. A., et al., Measurements of stratospheric carbon dioxide and water vapor at northern midlatitudes: Implications for troposphere-to-stratosphere transport, *Geophys. Res. Lett.*, *22*, 2737-2740, 1995.

Boering, K. A., S. C. Wofsy, B. C. Daube, H. R. Schneider, M. Loewenstein, J. R. Podolske, and T. J. Conway, Stratospheric mean ages and transport rates from observations of carbon dioxide and nitrous oxide, *Science*, *274*, 1340-1343, 1996.

Brewer, A. W., Evidence for a world circulation provided by the measurements of helium and water vapor distribution in the stratosphere, *Q. J. R. Meteorol. Soc.*, *75*, 351-363, 1949.

Conway, T. J., P. P. Tans, L. S. Waterman, K. W. Thoning, D. R. Kitzis, K. A. Masarie, and N. Zhang, Evidence for interannual variability of the carbon cycle from the National Oceanic and Atmospheric Administration/ Climate Monitoring and Diagnostics Laboratory global air sampling network, *J. Geophys. Res.*, *99*, 22,831-22,855, 1994.

Dessler, A. E., A reexamination of the "stratospheric fountain" hypothesis, *Geophys. Res. Lett.*, *25*, 4165-4168, 1998.

Dessler, A. E., E. M. Weinstock, E. J. Hintsa, J. G. Anderson, C. R. Webster, R. D. May, J. W. Elkins, and G. S. Dutton, An examination of the total hydrogen budget of the lower stratosphere, *Geophys. Res. Lett.*, *21*, 2563-2566, 1994.

Dobson, G. M. B., Origin and distribution of the polyatomic molecules in the atmosphere, *Proc. R. Soc. London, Ser. A*, *236*, 187-193, 1956.

Ehhalt, H. D., P. E. Röth, and U. Schmidt, On the temporal variation of stratospheric trace gas concentrations, *J. Atmos. Chem.*, *1*, 27-51, 1983.

Elkins, J. W., et al., Airborne gas chromatograph for in situ measurements of long-lived species in the upper troposphere and lower stratosphere, *Geophys. Res. Lett.*, *23*, 347-350, 1996.

Eluszkiewicz, J., et al., Residual circulation in the stratosphere and lower mesosphere as diagnosed from Microwave Limb Sounder data, *J. Atmos. Sci.*, *53*, 217, 1996.

Graedel, T. E., chair, *Atmospheric Effects of Stratospheric Aircraft*, National Academy Press, Washington, D. C., 1994.

Hall, T. M., and R. A. Plumb, Age as a diagnostic of stratospheric transport, *J. Geophys. Res.*, *99*, 1059-1070, 1994.

Hall, T. M., and D. W. Waugh, Timescales for the stratospheric circulation derived from tracers, *J. Geophys. Res.*, *102*, 8891-9001, 1997a.

Hall, T. M., and D. W. Waugh, Tracer transport in the tropical stratosphere due to vertical diffusion and horizontal mixing, *Geophys. Res. Lett.*, *24*,1383-1386, 1997b.

Harnisch, J., R. Borchers, P. Fabian, and M. Maiss, Tropospheric trends for CF_4 and C_2F_6 since 1982, derived from SF_6 dated stratospheric air, *Geophys. Res. Lett.*, *23*, 1099-1102, 1996.

Herman, R. L., et al., Tropical entrainment timescales inferred from stratospheric N_2O and CH_4 observations, *Geophys. Res. Lett.*, *25*, 2781-2784, 1998.

Hintsa, E. J., E. M. Weinstock, J. G. Anderson, R. D. May, and D. F. Hurst, On the accuracy of in situ water vapor measurements in the troposphere and lower stratosphere with the Harvard Lyman-α hygrometer, *J. Geophys. Res.*, in press, 1999.

Holton, J. R., P. H. Haynes, M. E. McIntyre, A. R. Douglass, R. B. Rood, and L. Pfister, Stratosphere-troposphere exchange, *Rev. Geophys.*, *33*, 405-439, 1995.

Hurst, D. F., et al., Closure of the total hydrogen budget of the northern extratropical lower stratosphere, *J. Geophys. Res.*, in press, 1999.

Keeling, C. D., et al., *Aspects of Climate Variability in the Pacific and Western Americas*, Ed. *Geophys. Monog.*, vol. 55, edited by D. H. Peterson, AGU, pp. 165 - 236, Washington, DC, 1989.

Kida, H., General circulation of air parcels and transport characteristics derived from a hemispheric GCM, 2, Very long term motions in the troposphere and stratosphere, *J. Meteorol. Soc. Jpn.*, *61*, 510-522, 1983.

Kley, D., A. Schmeltekopf, K. Kelly, R. Winkler, T. Thompson, and M. McFarland, The U-2 Lyman-Alpha results from the 1980 Panama Experiment, in *The Stratospheric-Tropospheric Exchange Experiment*, edited by A. P. Margozzi, pp. 82-125, *NASA tech. memo. 84297*, U.S. Gov. Print Office, Washington, D. C., 1983.

Matsueda, H., and H. Y. Inoue, Measurements of atmospheric CO_2 and CH_4 using a commercial airliner from 1993 to 1994, *Atmos. Environ.*, *30*, 1647-1655, 1996.

Minschwaner, K., A. E. Dessler, J. W. Elkins, C. M. Volk, D. W. Fahey, M. Loewenstein, J. R. Podolske, A. E. Roche, and K. R. Chan, The bulk properties of isentropic mixing into the tropics in the lower stratosphere, *J. Geophys. Res.*, *101*, 9433-9439, 1996.

Mote, P. W., K. H. Rosenlof, R. S. Harwood, J. R. Holton, and J. W. Waters, Seasonal variations of water vapor in the tropical lower stratosphere, *Geophys. Res. Lett.*, *22*, 1093-1096, 1995.

Mote, P. W., K. H. Rosenlof, M. E. McIntyre, E. S. Carr, J. C. Gille, J. R. Holton, J. S. Kinnersley, H. C. Pumphrey, J. M. Russell III, and J. W. Waters, An atmospheric tape recorder: The imprint of tropical tropopause temperatures on stratospheric water vapor, *J. Geophys. Res.*, *101*, 3989-4006, 1996.

Mote, P. W., T. J. Dunkerton, M. E. McIntyre, E. A. Ray, P. H. Haynes, and J. M. Russell III, Vertical velocity, vertical diffusion, and dilution by midlatitude air in the tropical lower stratosphere, *J. Geophys. Res.*, *103*, 8651-8666, 1998.

Nakazawa, T., K. Miyashita, S. Aoki, and M. Tanaka, Temporal and spatial variations of upper tropospheric and lower stratospheric carbon dioxide, *Tellus, Ser. B*, *43*, 106-107, 1991.

Newell, R. E., and S. Gould-Stewart, A stratospheric fountain? *J. Atmos. Sci.*, *38*, 2789-2796, 1981.

Randel, W. J., F. Wu, J. M. Russell III, A. Roche, and J. W. Waters, Seasonal cycles and QBO variations in stratospheric CH_4 and H_2O observed in *UARS* HALOE data, *J. Atmos. Sci.*, *55*, 163-185, 1998.

Rosenlof, K. H., Seasonal cycle of the residual mean circulation in the stratosphere, *J. Geophys. Res.*, *100*, 5173-5191, 1995.

Schmidt, U., and A. Khedim, *In situ* measurements of carbon dioxide in the winter Arctic vortex and at midlatitudes: An indicator of the "age" of stratospheric air, *Geophys. Res. Lett.*, *18*, 763-766, 1991.

Stolarski, R. S. and H. L. Wesoky, (Eds.), The atmospheric effects of stratospheric aircraft: A fourth program report, *NASA Ref. Publ., 1359*, 1995.

Trepte, C. R., and M. H. Hitchman, Tropical stratospheric circulation deduced from satellite aerosol data, *Nature, 355*, 626-628, 1992.

Volk, C. M., et al., Quantifying transport between the tropical and mid-latitude lower stratosphere, *Science*, *272*, 1763-1768, 1996.

Weinstock, E. M., E. J. Hintsa, A. E. Dessler, J. F. Oliver, N. L. Hazen, J. N. Demusz, N. T. Allen, L. B. Lapson, and J. G. Anderson, A new fast-response photofragment fluorescence hygrometer for use on the ER-2 and Perseus remotely piloted aircraft, *Rev. Sci. Instrum.*, *65*, 3544- 3554, 1994.

Webster C. R., R. D. May, C. A. Trimble, R. G. Chave, and J. Kendall, Aircraft (ER-2) laser infrared absorption spectrometer (ALIAS) for *in situ* stratospheric measurements of HCl, N_2O, CH_4, NO_2, and HNO_3.

A. E. Andrews, B. C. Daube, and S. C. Wofsy, Department of Earth and Planetary Sciences and the Division of Engineering and Applied Sciences, Harvard University, Cambridge, MA 02138. (aea@io.harvard.edu, bcd@io.harvard.edu, scw@io.harvard.edu.)

K. A. Boering, Departments of Chemistry and of Geology and Geophysics, University of California, Berkeley, CA 94720. (boering@cchem.berkeley.edu.)

T. P. Bui, NASA Ames Research Center, Moffett Field, CA 94035-1000. (pbui@mail.arc.nasa.gov.)

E. J. Hintsa, Department of Marine Chemistry and Geochemistry, Woods Hole Oceanographic Institution, Woods Hole, MA 02543. (ehintsa@whoi.edu.)

E. M. Weinstock, Department of Chemistry and Chemical Biology, Harvard University, Cambridge, MA 02138. (weinstock@huarp.harvard.edu.)

(Received December 4, 1998; revised February 22, 1999; accepted March 1, 1999.)